Analytic evaluation of the thermal conductivity at the conditions of the powder bed fusion with electron beam (PBF-EB) additive manufacturing (AM) process

Available online at www.sciencedirect.com

ScienceDirect

Procedia CIRP 126 (2024) 585–590

www.elsevier.com/locate/procedia

17th CIRP Conference on Intelligent Computation in Manufacturing Engineering (CIRP ICME '23)

Analytic evaluation of the thermal conductivity at the conditions of the powder bed fusion with electron beam (PBF-EB) additive manufacturing (AM) process

Giovanni Rizza*, Manuela Galati, Paolo Antonioni, Luca Iuliano

Department of Management and Production Engineering (DIGEP), Integrated Additive Manufacturing center (IAM@PoliTo), Politecnico di Torino, Corso Duca degli Abruzzi 24, 10129 Torino, Italy

* Corresponding author. Tel.: +39 0110907280; *E-mail address:* giovannni.rizza@polito.it

Abstract

In the additive manufacturing powder bed fusion process with electron beam (PBF-EB) process, the thermal conductivity of the powder bed controls the interaction of the electron beam with the material, the heat transfer during the process, the cooling rate and, consequently, the final component microstructure. This property requires to be optimized, and the desired value is achieved at the present day only with a trial and error approach. This work proposes a numerical method that considers the powder bed's geometrical characteristics, including the neck formation among the powder particles. Examples of model applications are reported, considering the Ti6Al4V alloy processed with the PBF-EB process.

Keywords: Electron Beam Melting (EBM); Tortuosity; Sintering; Neck

1. Introduction

In the powder bed fusion with electron beam (PBF-EB) processes, thermal conductivity has a key role because it influences the interaction of the electron beam with powder material [1] and the heat transfer phenomena during the process. Thermal conductivity within a powder bed is described in the literature as the sum of three different contributions: diffusion, radiation and conduction phenomena [2]. In the case of the PBF-EB, thermal conductivity within partially sintered powder mainly occurs because of conduction. This is acceptable because the process occurs under a vacuum (convection is negligible [3]), and the contribution of radiation is an order of magnitude smaller than the conductive counterpart within solid material [4]. The evaluation of the thermal conductivity of the powder bed remains challenging because of the temperature evolution during the process and the evolution of the neck among the powder particles due to the sintering phenomena occurring at high temperatures.

At present day, the thermal conductivity of the powder material is mainly investigated by considering experimental or numerical approaches. An overview of the experimental approaches was proposed by Presley and Christensen [5]. Among the different experimental methods, some are specifically dedicated to the PBF-EB process. However, some of the methodologies proposed neglected the vacuum environment that characterizes the PBF-EB process [6]. Other works investigated the thermal conductivity at different temperatures but neglected the influence of the high temperature on the evolution in time of the neck that connects the powder particles [7,8].

10.1016/j.procir.2024.08.244

Among the different numerical models for thermal conductivity available in the literature, some are dedicated to additive manufacturing techniques [9–11]. Gusarov et al. [9] proposed a numerical model for the powder bed fusion with the laser beam process for polymers (PBF-LB/P). In this case, the thermal conductivity of bulk material was scaled according to the relative density of the powder bed, the coordination number, and the dimension of the neck between the powder particles. However, the geometrical information required to implement this model constrains the validity of this model to simplified structures of the powder bed, such as the simple cubic (SC), face centred cubic (FCC), or body centred cubic (BCC) structures, where these parameters are easy to measure. Chua et al. [10] implemented a finite element (FE) model consisting of a couple of powder particles in contact at a point to investigate the thermal conductivity as a function of the dimension of the bridge of material (neck) among the powder particles. The simulations were conducted considering processing conditions representative of the PBF-EB conditions: air at low pressure around the powder particles, powder particles with a diameter of 50 μm and a temperature that varied between 0.4 T_m and the solidus temperature of the material. The results obtained for a couple of powder particles were then extended to a powder bed by linear interpolation. The results obtained with such model are approximated because the effective geometry of the powder bed is neglected. To overcome such approximation in the case of micro PBF-LB/P, Grose et al. [11] used a PF simulation to predict the neck evolution during the process, and a FE model to perform a steady state heat transfer simulation and evaluate thermal conductivity. This methodology, however, is computationally expensive and requires several adjustments to move from the sintering simulation to the thermal conductivity. Moreover, the connection of phase field simulation to the AM process remains unclear, as the material parameters and the temperature evolution to set up the PF simulation were not provided.

In the case of a powder bed, determining the thermal conductivity of the solid fraction requires precise knowledge of the heat transfer region. For partially sintered powder particles, this area must consider a net of powder particles connected among each other. The concept of tortuosity may be adopted to describe the complexity of the path within the material. Tortuosity was introduced to describe the flow of a fluid through the void of a porous medium and was only recently proposed as a methodology to investigate the thermal or electrical diffusion phenomena in a porous material. Ahmadi et al. [12] proposed an approach based on volume averaging to evaluate the tortuosity of mono sized arrays of spheres. In this case, tortuosity was evaluated as a flow within the pores of the material. The methodology was adopted to evaluate the tortuosity of regular cubic and tetrahedral structures of spherical powder particles. The results were found to be in good agreement with both theoretical and experimental literature data. Montes et al. [13] proposed the evaluation of thermal tortuosity as the ratio between the sample length in the heat flux direction and the length of the shortest path within the solid material that connects the extremes of the sample. However, in the case of a powder substrate with low density, the dimension of the solid connection between the powder particles was neglected [13]. Leung et al. [14] used an analysis of the tortuosity factor to evaluate thermal conductivity. The value of the tortuosity factor was obtained using an open source application, TauFactor [15]. The inputs for the software are cross section images of the porous media that, in this case, were tomographies of the sintered powder bed. Then, ideally, a heat flux occurs on a sub-volume of the powder image. Heat flux is applied at the top of the picture, and the thermal flux is followed along the conductive phase. The results are strictly bonded to the image adopted for the evaluation, the dimension of the inlet area and the balance between the phases of the system. Moreover, the sintered test samples are not representative of the evolution of the sintering process during the PBF-EB.

The current work proposes a novel methodology to evaluate the tortuosity factor and the thermal conductivity in a powder bed. Information about the temperature evolution that characterizes the PBF-EB process and the subsequent evolution of the neck radius among the powder particles were coupled to a novel methodology based on the concept of tortuosity. The proposed methodology attempted to overcome the limitations of the currently available literature.

2. Methodology

The thermal conductivity of a powder bed can be evaluated by scaling the thermal diffusivity of the powder, as reported in equation (1) [8]

$$\lambda_{pow} = \alpha_{pow}\rho_{pow}c_p \quad (1)$$

Where α_{pow} represents the thermal diffusivity of the powder material, ρ_{pow} represents the density of the powder bed, and c_p represents the specific heat capacity of the powder bed.
ρ_{pow} can be evaluated as $\rho_{pow}=\rho_0 n$, where ρ_0 is the theoretical density of the bulk material considered and n represents the volume fraction of the solid material within the considered domain.
α_{pow} can be expressed as reported in equation (2) [14]

$$\alpha_{pow} = \alpha_0 \frac{n}{\tau} \quad (2)$$

in which α_0 represents the thermal diffusivity of the bulk material and τ represents the tortuosity of the system.

In this work, the evaluation of τ is extracted from Ahmadi et al. [12]. In their formulation, the porous media consisted of a solid powder material immersed in a fluid. The tortuosity represented the geometrical complexity of the path followed by the fluid through the pores. In the case of a powder bed going under sintering, the net formed by sintered particles in which the heat transfer occurs and where the thermal conductivity should be evaluated may be assumed as porous material immersed in a liquid that travels along the channels created by the necks. therefore, the concept of tortuosity is modified to consider the heat flux as a fluid going through the continuous path created by the necks among the particles. The

formulation of τ reported in equation (3) was formalized under the following hypothesis:

- The porous material is made of two phases: a persistent solid phase and the void space between the solid particles.
- The solid phase is distributed heavenly over the domain.
- The phase where the flux occurs should be connected. This means that any two points inside the conducting phase should be linked by a curve that is entirely contained within the conducting phase.

$$\tau = \sqrt{\frac{n^2 d_p^2}{36(1-n)^2} \frac{\left(2+T_f^*\right)}{3{\Delta_f}^2 T_f^*}} \tag{3}$$

For the definition of the quantities presented in equation (3), an elementary volume (REV) was identified. The main characteristic of the REV is that the distribution of the solid material and the void is statistically representative of the powder bed. In particular, n represents the volume fraction of the solid material with respect to the total volume (equation (4)); Δ_f represents the hydraulic radius defined as the ratio of the volume of the solid material and the void-solid interface area (equation (5)). T_f* represents the tortuosity tensor of the fraction of volume occupied by the solid material. For an isotropic medium, this can be written as in equation (6), where δ_{ij} is the Kronecker delta function and θ^S=S_{ss}/S_0.

$$n = \frac{U_{0S}}{U_0} \tag{4}$$

$$\Delta_f = \frac{U_{0S}}{S_{fs}} \tag{5}$$

$$T_f^* = \frac{\theta^S}{n}\delta_{ij} = \frac{S_{SS}U_0}{S_0 U_{0S}}\delta_{ij} \tag{6}$$

In equation (4) U_{0S} represents the volume of the solid material within the REV and U_0 represents the total volume of the REV. In equation (5) S_{fs} represents the area of the interface between the solid material and the vacuum inside the REV. In equation (6) S_{SS} represents the area of the material that crosses the REV boundaries while S_0 represents the total lateral surface of the REV. U_0 and S_0 were evaluated as the volume and surface, respectively, of the minimum convex polygon or convex hull [16] that contains all the centres of the powder particles and represents the REV. Assuming a generic REV, the volume of the solid phase contained on the inside is evaluated as reported in equation (7)

$$U_{0S} = \iint_{D_{0S}} f(x,y)\, dD_{0S} \tag{7}$$

where f(x,y) is a generic function that describes the solid material. The integration domain D_{0s} represents the solid material inside the REV. The interface area of solid material to the void, S_{fs} is evaluated as reported in equation (8), assuming that the geometry of the solid material is axisymmetric.

$$S_{fS} = \vartheta \int_a^b f(x) \cdot (1 + (f'(x)^2) dx \tag{8}$$

where ϑ is the rotation angle, a and b represent the extreme of integration and f(x) represents the function that describes the profile of the solid material.

Finally, the area of the solid material that crosses the REV (S_{ss}) is defined as in equation (9).

$$S_{SS} = \int_a^b f(x) dx \tag{9}$$

As can be observed, with this definition, the tortuosity factor (equation (3)) is only determined by describing the geometry of the powder bed. All these features evolve with the sintering process varying with the time and the temperature. The track of the variation of these features is obtained by phase field simulations.

3. Results and Discussion

The methodology presented in section 2 was applied to a REV made of a simple cubic structure. This was composed of eight powder particles that sinter at the PBF-EB conditions. Powder particles were assumed to have a diameter of 80 μm, and each centre of the particle was assumed to be located in a vertex of the cube. Fig. 1 reports a representation of the REV adopted. The material considered for this simple application case was Ti6Al4V.

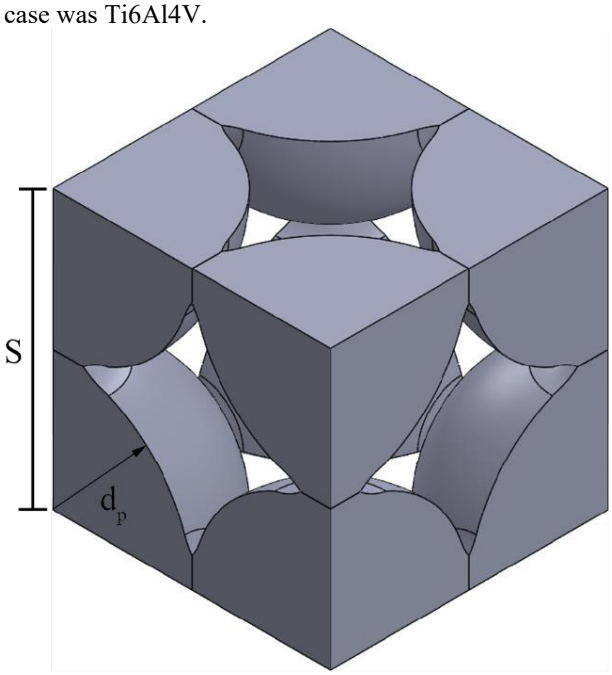

Fig. 1: REV adopted for the evaluation of the geometrical quantities of the simple cubic structure.

The ordered structure is symmetric to all the coordinate planes. Fig. 2 represents a portion of the REV consisting of an eighth of a powder particle, a quarter of a half neck and the reference system adopted for the evaluation of the geometric quantities for the tortuosity factor.

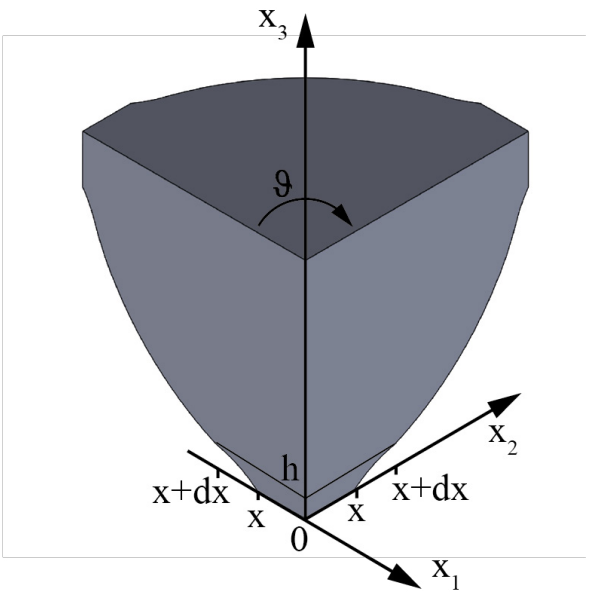

Fig. 2: Portion of the REV and the reference system adopted for the evaluation of geometrical quantities.

The total volume and the total lateral surface of the REV are evaluated considering the convex hull geometry with vertices placed at the centre of the powder particles.

U_{0S} is obtained as the sum of the volume of the sphere that represents the powder particle and the volume enclosed within a hyperboloid of one sheet that approximates the geometry of the neck. The calculation of the volume is reported in equation (10)

$$U_{0S} = 8\iint_{D_1}\sqrt{R^2 - x_1^2 - x_2^2}\,dx_1dx_2 - 24\iint_{D_2}\sqrt{R^2 - x_1^2 - x_2^2}\,dx_1dx_2 + 24\iint_{D_2} c\sqrt{\frac{x_1^2+x_2^2}{x^2} - 1}\,dx_1dx_2 \quad (10)$$

The integration domains are detailed in equations (11) and (12)

$$D_1 = \left\{(x_1, x_2) \in \mathbb{R} : -R < x_1 < 0;\ 0 < x_2 < \sqrt{R^2 - x_1^2}\right\} \quad (11)$$

$$D_2 = \left\{(x_1, x_2) \in \mathbb{R} : -R < x_1 < -R + h;\ 0 < x_2 < \sqrt{R^2 - x_1^2}\right\} \quad (12)$$

where R represents the radius of the powder particle, h represents the height of half hyperboloid, and x is the semiaxes of the hyperboloid and is considered equal to the neck radius. c is the semi focal distance equal to $c = a\sqrt{2}$

S_{fs} is evaluated as in equation (13). This is obtained as the sum of the surfaces of a sphere representing the powder particle and a hyperboloid representing the neck between the powder particles.

$$S_{fS} = 8 \times \frac{\pi}{2}\int_{-R+h}^{-(x+dx)} \sqrt{R^2 - x_3^2} \times \left(1 + \left(\frac{-x_3}{\sqrt{R^2 - x_3^2}}\right)^2\right) dx_3 + 24 \times \frac{\pi}{2}\int_0^h b\sqrt{\frac{x_3^2}{x^2} - 1} \times \left(1 + \left(\frac{\frac{b}{x^2}x_3^2}{\sqrt{\frac{x_3^2}{x^2} - 1}}\right)^2\right) dx_3 \quad (13)$$

where x represents the neck radius, while (x+dx) is the radius of the neck at the point of curvature change, moving from the surface of the powder particle to the surface of the neck. R is the radius of the powder particle, while h is the distance between the middle plane of the neck and the point of curvature change. These quantities are reported in Fig. 2. S_{SS} is evaluated according to equation (14)

$$S_{SS} = 24\int_0^x R dx_3 + 24\int_x^{x+dx} b\sqrt{\frac{x_3^2}{x^2} - 1}dx_3 + 24\int_{x+dx}^{R-h}\sqrt{R^2 - x_3^2}dx_3 + 24\int_{R-h}^{R} b\sqrt{\frac{x_3^2}{x^2} - 1}dx_3 \quad (14)$$

The evolution in time of the neck among the powder particles was obtained with the phase field methodology proposed by Rizza et al. [17].

Table 1 summarizes the geometrical information, the values of U_{0s}, S_{fs} and S_{SS} and the value of tortuosity evaluated at every second of the simulation. The values of U_0 = 512000 μm³ and S_0 = 38400 μm² were obtained as volume and surface, respectively, of the convex hull geometry corresponding to the REV under consideration.

Table 1: Geometrical data of the neck, results of the calculation of equations (46), (49) and (50) for the REV considered and tortuosity obtained at each step of the simulation.

time	Temp	x	x+dx	h	U_{0S}	S_{fs}	S_{SS}	τ
[s]	[K]	[μm]	[μm]	[μm]	[μm³]	[μm²]	[μm²]	[-]
0.5	879	3.84	7.02	0.80	267750	19344	30530	0.89
1.5	913	5.40	9.01	1.40	267153	19479	31150	0.90
2.5	964	6.31	10.08	1.78	266764	19966	31570	0.92
3.5	1016	6.80	12.40	2.18	267477	20422	30984	0.94
4.5	1050	7.28	10.79	1.87	268141	20769	32174	0.95
5.5	1101	7.48	12.33	2.42	266871	21262	31706	0.97
6.5	1153	7.95	13.48	2.53	268765	21941	31619	1.01
7.5	1187	8.19	14.35	2.89	268237	22591	31496	1.04
8.5	1239	8.42	15.24	3.10	268994	23183	31334	1.08
9.5	1273	8.62	16.02	3.54	267492	24065	31240	1.11

Table 2 summarizes the values of thermal diffusivity of the bulk material (α_0), specific heat capacity(c_p), the density of the bulk (ρ_0) and powder (ρ_{pow}) material, adopted for the calculation of the thermal diffusivity and conductivity of the powder material. All the bulk material properties were assumed to be temperature dependent, varying according to the system's temperature at each simulation step. The bulk material's thermal conductivity and specific heat capacity were retrieved from Qi et al. [18]. No information is available

in the literature about the evaluation of the specific heat capacity (c_p) and the density of the powder bed (ρ_{pow}). In the current work, c_p was assumed to be equal to that of the bulk material [19–21]. ρ_{pow} was obtained by scaling the density of the bulk material according to the fraction of solid material within the REV. The thermal diffusivity of the bulk material was evaluated according to equation (15)

$$\alpha_0 = \frac{\lambda_0}{\rho_0 c_p} \quad (15)$$

Table 2: Values of thermal diffusivity of the bulk material (α_0), specific heat capacity (c_p), the density of the bulk material (ρ_0) and density of the powder (ρ_{pow}), adopted for the evaluation of the thermal diffusivity and conductivity of the powder.

Time	Temperature	α_0	c_p	ρ_0	ρ_{pow}
[s]	[K]	[m^2s^{-1}]	[$Jkg^{-1}K^{-1}$]	[kgm^{-3}]	[kgm^{-3}]
0.5	879	2.95×10^{-6}	912.53	4273.69	2234.92
1.5	913	2.99×10^{-6}	937.61	4262.54	2224.13
2.5	964	3.05×10^{-6}	975.24	4245.81	2212.17
3.5	1016	3.11×10^{-6}	1013.61	4228.75	2209.17
4.5	1050	3.14×10^{-6}	1038.69	4217.60	2208.82
5.5	1101	3.20×10^{-6}	1076.32	4200.87	2189.64
6.5	1153	3.25×10^{-6}	1114.68	4183.82	2196.22
7.5	1187	3.28×10^{-6}	1139.77	4172.66	2186.07
8.5	1239	5.31×10^{-6}	736.80	4155.61	2183.27
9.5	1273	5.43×10^{-6}	743.6	4144.46	2165.25

Table 16 summarises the values of thermal diffusivity (α_{pow}) and conductivity (λ_{pow}) of the REV considered. These values are obtained at each simulation step corresponding to the temperature of the powder bed.

Table 3: Thermal diffusivity (α_{pow}) and thermal conductivity (λ_{pow}) of the powder material for every second of the simulation.

Time	Temperature	α_{pow}	λ_{pow}
[s]	[K]	[m^2s^{-1}]	[$Wm^{-1}K^{-1}$]
0.5	879	1.72×10^{-6}	3.50
1.5	913	1.74×10^{-6}	3.63
2.5	964	1.74×10^{-6}	3.75
3.5	1016	1.72×10^{-6}	3.85
4.5	1050	1.73×10^{-6}	3.96
5.5	1101	1.71×10^{-6}	4.03
6.5	1153	1.68×10^{-6}	4.11
7.5	1187	1.65×10^{-6}	4.10
8.5	1239	2.60×10^{-6}	4.18
9.5	1273	2.55×10^{-6}	4.11

4. Conclusions

The current work proposes a novel methodology to evaluate thermal conductivity at the PBF-EB conditions. Information about the temperature evolution that characterizes the PBF-EB process and the subsequent evolution of the neck radius among the powder particles were coupled to a novel methodology based on the concept of tortuosity. The proposed methodology was applied to a simple cubic structure made of eight powder particles with the same diameter. For this structure, thermal conductivity was found to vary between 3.50 $Wm^{-1}K^{-1}$ and 4.11 $Wm^{-1}K^{-1,}$ and these values were found to be an order of magnitude smaller than the thermal conductivity of the bulk material. The data obtained using the methodology proposed in the current work were found in good agreement with the thermal conductivity obtained by Zhang et al. [22] and Liu et al. [23]. The slight differences in the numerical values are related to the simple geometry considered in the current work, while the Zhang et al. [22] and Liu et al. [23] considered an experimental approach. An improvement in the accuracy of the numerical values could be obtained by considering a REV with powder particles with a powder size distribution more representative of the PBF-EB process.

References

[1] Luo Z, Zhao Y. A survey of finite element analysis of temperature and thermal stress fields in powder bed fusion Additive Manufacturing. Addit. Manuf. 2018 21 318–332.

[2] Hsu CT, Cheng P, Wong KW. Modified Zehner-Schlunder models for stagnant thermal conductivity of porous media. Int. J. Heat Mass Transf. 1994 37 2751–2759.

[3] Galati M, Iuliano L, Salmi A, Atzeni E. Modelling energy source and powder properties for the development of a thermal FE model of the EBM additive manufacturing process. Addit. Manuf. 2017 14 49–59.

[4] Zhao Y, Koizumi Y, Aoyagi K, Yamanaka K, Chiba A. Thermal properties of powder beds in energy absorption and heat transfer during additive manufacturing with electron beam. Powder Technol. 2021 381 44–54.

[5] Presley MA, Christensen PR. Thermal conductivity measurements of particulate materials 1. A review. J. Geophys. Res. E Planets. 1997 102 6535–6549.

[6] Neira Arce A. Thermal Modeling and Simulation of Electron Beam Melting for Rapid Prototyping on Ti6Al4V Alloys, North Carolina State University, 2012. https://www.proquest.com/docview/1345924365/abstract/3E37C3575D824C4EPQ/1?accountid=28840.

[7] Gong X, Cheng B, Price S, Chou K. Powder-bed electron-beam-melting additive manufacturing: powder characterization, process simulation and metrology. Early Career Tech. Conf. Birmingham, AL. 2013 55–66.

[8] Smith CJ, Tammas-Williams S, Hernandez-Nava E, Todd I. Tailoring the thermal conductivity of the powder bed in Electron Beam Melting (EBM) Additive Manufacturing. Sci. Rep. 2017 7 1–8.

[9] Gusarov A V., Laoui T, Froyen L, Titov VI. Contact thermal conductivity of a powder bed in selective laser sintering. Int. J. Heat Mass Transf. 2003 46 1103–1109.

[10] Chua BL, Lee HJ, Ahn DG. Estimation of Effective Thermal Conductivity of Ti-6Al-4V Powders for a Powder Bed Fusion Process Using Finite Element Analysis. Int. J. Precis. Eng. Manuf. 2018 192. 2018 19 257–264.

[11] Grose J, Cullinan M, Dibua OG, Behera D, Foong CS. Simulation and Characterization of Nanoparticle Thermal Conductivity for a

Microscale Selective Laser Sintering System. Proc. ASME 2021 16th Int. Manuf. Sci. Eng. Conf. MSEC 2021. 2021 2.

[12] Ahmadi MM, Mohammadi S, Hayati AN. Analytical derivation of tortuosity and permeability of monosized spheres: A volume averaging approach. Phys. Rev. E - Stat. Nonlinear, Soft Matter Phys. 2011 83 1–8.

[13] Montes JM, Cuevas FG, Cintas J. Electrical and thermal tortuosity in powder compacts. Granul. Matter. 2007 9 401–406.

[14] Leung CLA, Tosi R, Muzangaza E, Nonni S, Withers PJ, Lee PD. Effect of preheating on the thermal, microstructural and mechanical properties of selective electron beam melted Ti-6Al-4V components. Mater. Des. 2019 174 107792.

[15] Cooper SJ, Bertei A, Shearing PR, Kilner JA, Brandon NP. TauFactor: An open-source application for calculating tortuosity factors from tomographic data. SoftwareX. 2016 5 203–210.

[16] Mordukhovich BS, Mau Nam N. Convex Analysis and Beyond Springer International Publishing, Cham, 2022.

[17] Rizza G, Galati M, Iuliano L. A phase-field study of neck growth in electron beam powder bed fusion (EB-PBF) process of Ti6Al4V powders under different processing conditions. Int. J. Adv. Manuf. Technol. 2022 123 855–873.

[18] Qi HB, Yan YN, Lin F, Zhang RJ. Scanning method of filling lines in electron beam selective melting. Proc. Inst. Mech. Eng. Part B J. Eng. Manuf. 2007 221 1685–1694.

[19] Zäh MF, Lutzmann S. Modelling and simulation of electron beam melting. Prod. Eng. 2010 4 15–23.

[20] Shen N, Chou K. Thermal Modeling of Electron Beam Additive Manufacturing Process: Powder Sintering Effects. ASME 2012 Int. Manuf. Sci. Eng. Conf. Collocated with 40th North Am. Manuf. Res. Conf. Particip. with Int. Conf., MSEC 2012. 2013 287–295.

[21] Sih SS, Barlow JW. The Prediction of the Emissivity and Thermal Conductivity of Powder Beds. Http://Dx.Doi.Org/10.1080/02726350490501682. 2010 22 427–440.

[22] Zhang S, Lane B, Whiting J, Chou K. An investigation into metallic powder thermal conductivity in laser powder bed fusion additive manufacturing, in: Solid Free. Fabr. 2018 Proc. 29th Annu. Int. Solid Free. Fabr. Symp. - An Addit. Manuf. Conf. SFF 2018, 2020: pp. 1796–1807.

[23] Liu M, Chiu LNS, Shen H, Fang X, Tao Z, Huang A, Davies C, Wu X, Yan W. Effective thermal conductivities of metal powders for additive manufacturing. Powder Technol. 2022 401 117323.